IET Optoelectronics

Research Article

IET Journals
The Institution of Engineering and Technology

Investigating channel frequency selectivity in indoor visible-light communication systems

ISSN 1751-8768
Received on 12th February 2015
Revised on 16th June 2015
Accepted on 7th July 2015
doi: 10.1049/iet-opt.2015.0015
www.ietdl.org

Shihe Long[1], Mohammad Ali Khalighi[1] ✉, Mike Wolf[2], Salah Bourennane[1], Zabih Ghassemlooy[3]

[1]*Institut Fresnel, UMR CNRS 7249, École Centrale Marseille, Marseille, France*
[2]*Communications Research Laboratory, Ilmenau University of Technology, Ilmenau, Germany*
[3]*Optical Communications Research Group, NCR Lab, Faculty of Engineering and Environment, Northumbria University, Newcastle upon Tyne, UK*
✉ *E-mail: Ali.Khalighi@fresnel.fr*

Abstract: Channel characterisation for indoor visible-light communication systems is revisited. The purpose of this study is to evaluate the channel frequency selectivity, or in other words, the significance of inter-symbol interference (ISI) at the receiver and the necessity of channel equalisation to recover the transmitted data. The authors focus on the effect of the indoor channel by assuming no bandwidth constraint on the light-emitting-diodes and by considering a simple intensity modulation technique, excluding discrete multi-tone modulation. The channel impulse response (CIR) is first simulated using the iterative site-based method. Then, conventional metrics for evaluating channel frequency selectivity, that is, the root-mean-square delay spread and channel frequency response are investigated and their practical interest is discussed. The authors also consider the signal-to-ISI ratio (SIR), which they define based on the sampled (i.e. discrete-time) signal at the receiver, and demonstrate its usefulness in determining the necessity of channel equalisation at the receiver. They consider several link scenarios in a medium-size and a large room, and show the significance of the LOS components of CIR in determining the channel frequency selectivity. They also discuss the choice of the receiver filter and explain how it affects the SIR.

1 Introduction

Visible-light communications (VLC) have attracted particular attention in the research world due to their potential in providing very high-rate data transmission through the use of solid-state lighting devices, especially in indoor environments [1, 2]. VLC offer several advantages over the 'traditional' radio-frequency (RF) wireless technologies (e.g. WiFi connections) including the availability of a very large unlicensed spectrum (about hundreds of THz), spatial confinement leading to communication security, and immunity to RF interference. Moreover, by exploiting the already-installed light-emitting-diode (LED) lighting infrastructures for broadband data transmission, VLC can be considered as a good example of green communication for the next generation high-speed local area networks.

The main constraint on the data rate in VLC systems arises from the limited bandwidth of commercially available LEDs. The 'classical' approach is to use separate red–green–blue (RGB) emitters and to combine them to produce white light. However, this approach is of limited use and is phasing out in the lighting industry due to difficulties in RGB balancing and the high cost, although it provides devices of relatively high bandwidth (a few tens of MHz) and gives the possibility of colour mixing [3]. A popular alternative to RGB lighting is to use the so-called white LEDs, where a blue LED is used together with yellowish phosphor coating to emit broad spectrum white light. The main drawback of commercial white LEDs is their slow modulation response due to the slow response time of the phosphorous that limits the modulation bandwidth of the device to a few MHz. One proposed solution is to use a blue filter at the receiver to remove this slow component from the modulated signal such that the modulation bandwidth can be increased. For instance, it was shown in [4] that the 6 dB modulation bandwidth can be increased to more than 170 MHz provided that the LED driver circuit is well designed. Very recently, researchers have considered the use of GaN-based micron-size LEDs (commonly called μLEDs) that have modulation bandwidths around 60 MHz [5, 6].

Over the past years, most of the research works have focused on increasing the data rate mainly by means of discrete multi-tone modulation (DMT) [7–12], and less attention has been devoted to the effect of the indoor channel and the limitations on the data rate that may arise from multipath propagation. As a matter of fact, DMT is a robust solution to the limited bandwidth of the LEDs and at the same time to the channel delay dispersion. Numerous experimental works have already demonstrated the potential of DMT to provide high data-rate VLC links [e.g. 13–15]. Although DMT has become very popular in VLC systems, its optimality is rather questionable, especially from the spectral and energy efficiency points of view. Compared with coherent field modulation, where two (optical) quadrature carriers are individually modulated, VLC based on DC-biased DMT suffers from a factor 2 bandwidth efficiency loss due to the intensity modulation constraint. If asymmetrically clipped DMT [16] is used to avoid the DC offset, the bandwidth efficiency is reduced by a further factor 2. Other disadvantages concern the requirement of highly linear LED-drivers, which have typically a low power efficiency. Furthermore, the bit error rate performance of DC-biased approaches is very sensitive to the clipping noise and the modulation index [17].

Some other modulation schemes have been under investigation recently such as pulse-amplitude modulation [18] and carrierless amplitude and phase modulation [19, 20] for use in VLC systems. While these schemes benefit from more implementation simplicity, they are more sensitive to channel delay dispersion as they do not benefit from the inherent dispersion mitigation property of DMT. Indeed, in some situations such as in relatively large rooms and under shadowed/blocked line-of-sight (LOS), the channel dispersion can be relatively large. In such cases, a channel equalisation step, implemented either in time or frequency domains, may be necessary at the receiver. The frequency-domain equalisation appears to be an interesting and relatively low-complexity solution as it effectively turns out to move the inverse fast-Fourier-transform (IFFT) operation (which is done at the transmitter in DMT-based signalling) to the receiver side [17, 18, 21].

Our purpose in this work is to quantify accurately the limitation arising from the indoor VLC multipath channel itself and to see in which situations it can effectively limit the transmission rate. In other words, we would like to investigate the limitation (arising solely from the channel) on the data rate before suffering from channel frequency selectivity, or in other words, inter-symbol interference (ISI). For this purpose, we will assume ideal optical components, for example, we neglect the bandwidth limitation of the LEDs, and focus on the optical channel and also exclude the case of DMT signalling. We simulate the aggregated channel impulse response (CIR) including both LOS and diffuse components by using the well-known iterative site-based method [22]. To investigate the channel frequency selectivity, we consider the channel delay dispersion, frequency response, and also the signal-to-ISI ratio (SIR). We show that the main factor that impacts the channel frequency selectivity is the asymmetry between the multiple LOS paths corresponding to the multiple LED emitters rather than multipath reflections. Moreover, we clarify the role of the receiver filter and its real impact on the ISI after signal sampling.

The rest of the paper is organised as follows. We present the channel model and the simulation method that we use to obtain the CIR in Section 2. The definitions of different channel characterisation metrics including the SIR are provided in Section 3. Then, we state in Section 4 our main assumptions and describe the system configuration for the case studies that we consider in this paper. Next, some simulation-based numerical results are presented and discussed in Section 5 to study the VLC channel. Lastly, Section 6 concludes the paper.

2 Indoor optical channel modelling

In VLC systems, intensity modulation and direct detection (IM/DD) is used as the LED source is non-coherent. At the transmitter, the information-bearing signal is DC-biased prior to IM of the LED [see Fig. 1 (the DC bias sets the initial illumination level)]. At the receiver, a photo-diode (PD) followed by a trans-impedance amplifier (TIA) are used to regenerate the electrical signal, which is then passed through the receiver filter and sampled prior to signal demodulation. The role of the receiver filter, which can be a matched filter (MF) or a simple low-pass filter, is to reduce the noise effect.

Let us denote by $x(t)$ and $y(t)$ the emitted optical intensity at the transmitter and the generated photo-current at the output of the PD, respectively. We have

$$y(t) = \mathcal{R}x(t) \otimes h(t) + n(t) \tag{1}$$

where $\mathcal{R}$ is the PD responsivity in A/W, $h(t)$ is the baseband CIR, $\otimes$ denotes convolution, and $n(t)$ is the receiver noise, which is modelled as signal-independent additive white Gaussian noise (AWGN) with double-sided power spectral density (PSD) of $N_0/2$. $h(t)$ that includes the contribution of both the LOS and non-LOS (diffuse) components is given by

$$h(t) = \underbrace{\sum_{i=1}^{N_{\text{LED}}} V_i T(\phi_i) \frac{A_{\text{r}}(\varphi_i)}{d_i^2} \delta\left(t - \frac{d_i}{c}\right)}_{\text{LOS}} + \underbrace{\sum_{k=1}^{\infty} h^k(t)}_{\text{Diffuse}}. \tag{2}$$

Here $\delta(.)$ denotes the Dirac delta function, N_{LED} denotes the number of LED emitters, and V_i is the visibility function corresponding to the ith emitter, which is set to 0 when the LOS path between the receiver and the ith source is blocked, and to 1 otherwise. Moreover, ϕ_i and φ_i denote the emitting and incident angles, respectively, as illustrated in Fig. 2, $A_{\text{r}}(\varphi_i)$ is the effective receiving PD area, d_i is the link distance, c is the speed of light, and $T(\phi_i)$ is related to the ith source radiation pattern. Assuming Lambertian radiation pattern for LEDs, we have $T(\phi) = (m+1)\cos^m(\phi)/(2\pi)$, where m is the Lambertian order, which is related to the semi-angle at half power $\phi_{1/2}$ of the emitter: $m = -\ln 2/\ln(\cos(\phi_{1/2}))$. Note that in writing (2), we have implicitly assumed that the propagation delays between the electrical signals that modulate the different LEDs are negligible [7].

The calculation of diffuse component in (2) is far to be an easy task, and hence, simulation techniques are usually employed to obtain an approximation of $h^k(t)$.

As stated previously, in this work we have adopted the iterative site-based method for evaluating the non-LOS components. By this method, the inner surface of the room and the objects inside it are first decomposed into N tiny Lambertian reflecting elements with a given reflectivity. The k reflection response $h^{(k)}(t, S, R)$ for a given pair of source S (i.e. an LED or a reflecting surface) and receiver R (i.e. a surface or the PD) can be approximately evaluated as [22]

$$h^{(k)}(t, S, R) \simeq \sum_{n=1}^{N} \rho_{\varepsilon_n} h^{(k-1)}(t, S, \varepsilon_n^{\text{r}}) \otimes h^{(0)}(t, \varepsilon_n^{\text{s}}, R), \tag{3}$$

where ε_n^{r} and ε_n^{s} represent the nth element ε_n acting as a receiver and a source, respectively, and ρ_{ε_n} is the reflectivity of ε_n. Moreover, $h^{(0)}(t, \varepsilon_n^{\text{s}}, R)$ is the LOS CIR between the element n and R, which is simply a shifted Dirac delta function according to (2). This way, the convolution in (3) becomes rather a simple operation. Note that in order to reduce the simulation time, to determine the k-reflection response, we start by calculating $h^{(0)}(t, S, \varepsilon_n^{\text{r}})$ (which is quite simple to do), and use them to compute $h^{(1)}(t, S, \varepsilon_n^{\text{r}})$ according to (3). We repeat this procedure until we determine $h^k(t, S, \varepsilon_n^{\text{r}})$.

3 Channel characterisation metrics

We consider three criteria to quantify the limitation on the transmission rate: the root-mean-square (RMS) delay spread μ, the channel frequency response, and the SIR.

3.1 Conventional metrics

Two conventional channel characterisation metrics are the 3 dB cut-off frequency and μ. For instance, simulation results of channel delay spread were presented in [23], where the authors considered the wavelength dependence of the reflectivity of surfaces inside a room. Moreover, the channel frequency response was investigated in [7], where the integrating-sphere model [24] was used for the non-LOS component. Let us denote the channel frequency response by $H(f)$. The 3 dB channel cut-off frequency, $f_{-3\text{dB}}$ corresponds to

$$|H(f_{-3\text{dB}})|^2 = 0.5|H(0)|^2. \tag{4}$$

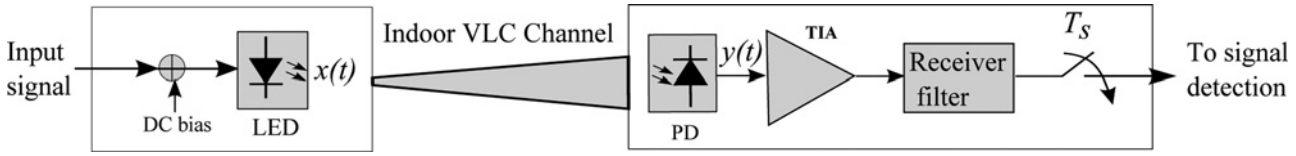

Fig. 1 *General block diagram of an IM/DD-based VLC system*

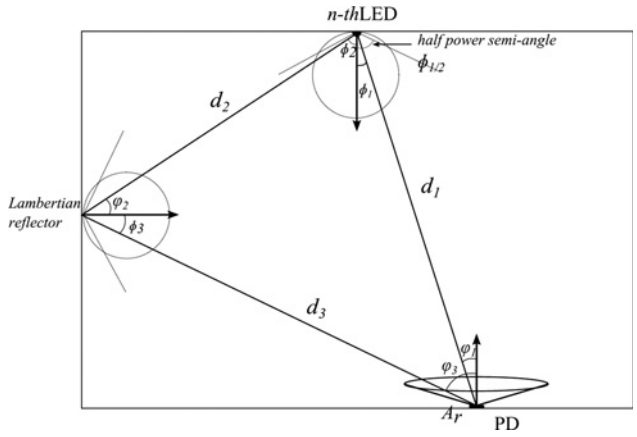

Fig. 2 *Propagation model for the indoor VLC channel*

However, because of the oscillating behaviour of the frequency response due to the presence of dominant LOS propagation components, this metric is of limited usage for determining the degree of channel frequency selectivity, as we will demonstrate in the next section.

The RMS delay spread is given by [25]

$$\mu = \left[\frac{\int_{-\infty}^{\infty}(t-\tau)^2 h^2(t)\,\mathrm{d}t}{\int_{-\infty}^{\infty} h^2(t)\,\mathrm{d}t}\right]^{1/2}, \tag{5}$$

where τ is the channel mean excess delay, defined as the square root of the second central moment of the CIR squared [25]

$$\tau = \frac{\int_{-\infty}^{\infty} th^2(t)\,\mathrm{d}t}{\int_{-\infty}^{\infty} h^2(t)\,\mathrm{d}t}. \tag{6}$$

3.2 Signal-to-ISI ratio

In the case of a relatively large μ, the link may suffer from ISI, which can seriously impact the system performance. We propose here to quantify the amount of ISI by defining the metric of SIR as

$$\mathrm{SIR} = \frac{P_{\mathrm{R,sig}}}{P_{\mathrm{R,ISI}}}, \tag{7}$$

where $P_{\mathrm{R,sig}}$ and $P_{\mathrm{R,ISI}}$ denote the received powers corresponding to the 'desired' signal and ISI, respectively. A high SIR corresponds to an almost frequency non-selective channel, whereas a relatively low SIR signifies the need to channel equalisation at the receiver. Let P_{R} be the total received power corresponding to a transmitted symbol. In some previous works (e.g. in [26]), $P_{\mathrm{R,sig}}$ is considered as the optical received power during the symbol period T_{s} and $P_{\mathrm{R,ISI}}$ as the received power outside T_{s}. In other words, it is assumed that

$$\begin{aligned} P_{\mathrm{R,sig}} &= P_{\mathrm{R}}(t \le T_{\mathrm{s}}), \\ P_{\mathrm{R,ISI}} &= P_{\mathrm{R}}(t > T_{\mathrm{s}}). \end{aligned} \tag{8}$$

Here we consider a more realistic definition for $P_{\mathrm{R,sig}}$ and $P_{\mathrm{R,ISI}}$ that is more appropriate for optical communication systems in practice. In fact, at the receiver, the electrical signal is filtered and then sampled prior to detection (see Fig. 1). Therefore, we should reasonably define the SIR after signal sampling. Let us consider the transmitted signal as follows

$$x(t) = \sum_j a_j g(t - jT_{\mathrm{s}}), \tag{9}$$

where a_k denotes the kth transmitted symbol [equal to zero or one for the case of non-return-to-zero (NRZ) on–off-keying (OOK) modulation, for example] and $g(t)$ is the pulse shaping filter. At the receiver, considering a sampling rate of $1/T_{\mathrm{s}}$ and assuming negligible noise $n(t)$, the signal corresponding to the time sample j is given by

$$y_j = a_j p(0) + \sum_{m \ne j} a_m p((j-m)T_{\mathrm{s}}), \tag{10}$$

where $p(t) = g(t) \otimes h(t) \otimes r(t)$ with $r(t)$ being the impulse response of the receiver filter. Note that in (10), a_j is the desired signal at time sample j and the right-hand-side term is in fact the ISI. We accordingly define the SIR as follows

$$\mathrm{SIR} = \frac{\mathrm{E}\{a_j^2\}[p(0)]^2}{\sum_{m \ne j} \mathrm{E}\{a_m^2\}[p((j-m)T_{\mathrm{s}})]^2}, \tag{11}$$

where E{.} stands for the expected value. Assuming power-normalised symbols and also normalised channel with respect to the main LOS path, (11) can be simplified as

$$\mathrm{SIR} = \frac{[p(0)]^2}{\sum_{m \ne j}[p((j-m)T_{\mathrm{s}})]^2}. \tag{12}$$

Note that in our simulations we consider $g(t)$ of a rectangular shape, which is quite rational for IM/DD signalling schemes. Concerning $r(t)$, we may consider the optimal MF at the receiver, which allows to maximise the signal-to-noise ratio (SNR) at the sampling times. However, the design of the MF becomes a complex task when we should deal with non-white noise (note that we consider here an analogue receiver filter and a sampling rate of one sample per symbol duration). For instance, if a large area PD (of relatively large capacitance) is used, the f^2 noise can be non-negligible [27]. This will necessitate a sharp roll-off of the filter transfer function in the stop-band. A suitable choice is then a Bessel filter (BF), which has a constant group delay in its pass-band. Alternatively, other filter types can be used such as a Butterworth filter, as suggested in [28], which has the advantage of providing a sharper transition between the pass-band and the stop-band for a given filter order, but causes a significant group delay distortion for high orders (typically larger than 7).

4 System configuration and assumptions

We describe in this section the configuration of the indoor VLC systems that we consider as the case study and also specify the corresponding assumptions and parameters. We first consider the case of a medium-size room as shown in Fig. 3. An array of (2 × 2) LEDs is considered, positioned on the ceiling as shown in Fig. 4*a*. We particularly study three receiver positions of R_1, R_2, and R_3 with coordinates (2.5, 2.5 m), (1.25, 1.25 m) and (0.5, 0.5 m), respectively, at a height of 0.85 m above the floor. Receivers are pointing upward (i.e. vertically towards the ceiling) and we do not consider any receiver lens. The reflecting surfaces of walls, floor, and the ceiling are assumed of plastic materials and as Lambertian reflectors of order 1. Note that, although the surface reflectivity is usually wavelength dependent, it is quite difficult to perform the simulations in the whole visible spectrum by considering this dependency, from the point of view of computational complexity. To simplify the simulations, we have used the results of Fig. 1 in [23] and calculated the average reflectivity over the entire visible spectrum. This is a good

IET Optoelectron., 2016, Vol. 10, Iss. 3, pp. 80–88

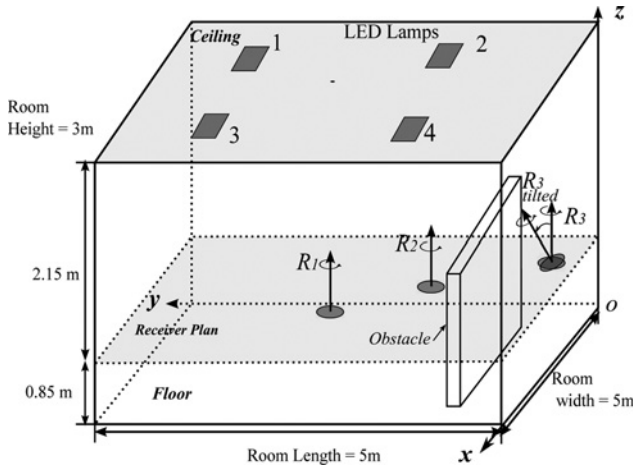

Fig. 3 *Indoor VLC system configuration in a medium-size room*

approximation if the maximum number of reflections considered in the simulations is not too high [23]. The calculated average reflectivities together with the other parameters adopted in our simulations are specified in Table 1.

We also consider two un-typical yet realistic situations: when all LOS paths are blocked by an obstacle, and when the receiver is tilted with respect to the vertical axis. For the blocked LOS case, we consider an obstacle of length, width, and height of 1.75, 0.25, and 2 m, respectively, at the origin coordinates (0.75, 0.25, 0 m) as shown in Fig. 3. The surface reflectivity of this obstacle is set to the same as of the wall. For the titled receiver case, we tilt the R_3 towards the centre of the ceiling by 30°.

Furthermore, in order to investigate the impact of the room size, we consider a relatively large room of dimension $(10 \times 10 \times 4)$ m^3 with an array of (4×4) LED lamps on the ceiling. The layout of the LED lamps for this case is shown in Fig. 4*b*. We investigate three receiver positions that we denote by R'_1, R'_2, and R'_3 at the coordinates (5, 5 m), (2, 2 m), and (0.5, 0.5 m), respectively.

To simulate the CIR, we assume that the same signal is transmitted from all LEDs. For the case of a small-to-medium size room, the use of several LEDs has the advantage of offering space diversity in the sense of avoiding signal loss in the case of (LOS) beam blocking. For the case of relatively large rooms or halls, this assumption applies to the case where VLC is used for information broadcasting. However, it is not adapted to multiple access applications where the use of cellular configurations seems to be a more appropriate approach [29]. In such a case, the CIR of each cell should be investigated individually, which would rather correspond to the presented study for the case of small-to-medium size room. Moreover, if multiple-input multiple-output configurations are to be used [30], spatial multiplexing is likely to be performed on different LED chips inside a lamp, while all LED lamps transmit the same

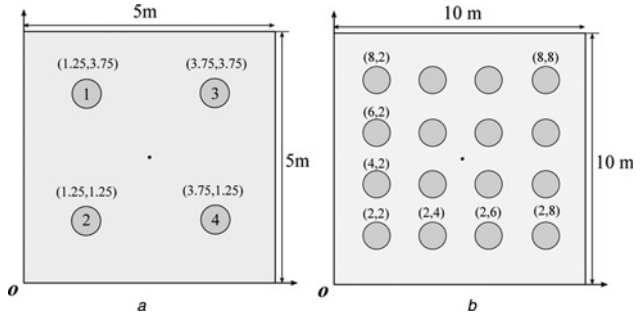

Fig. 4 *Layout of LEDs on the ceiling for the two cases of*
a Medium-size room of dimension $(5 \times 5 \times 3)$ m^3
b Large room of dimension $(10 \times 10 \times 4)$ m^3

Table 1 Simulation parameters

Parameter	Value
ceiling reflectivity	0.38
floor reflectivity	0.61
wall reflectivity	0.74
transmitter Lambertian order	1
receiver field-of-view (half angle)	70°
PD active area	1 cm^2

signals. As such, the results that we present in this paper will apply to this case as well.

Lastly, concerning the iterative site-based method that we use for simulating the CIR, we consider a maximum reflection order of 3. Indeed, as it is shown in [22], the power contribution by considering more reflections is practically negligible. The spatial resolution of the simulation method, that is, the area of each reflecting surface, is set to 10 cm × 10 cm. Moreover, the temporal resolution, that is, the bin width of the simulated CIR is set to 0.1 ns.

5 Numerical results

We present here some numerical results to investigate the optical propagation channel and the limitations arising from the channel on the maximum transmission rate. We investigate the three metrics of RMS delay spread, channel frequency response, and SIR, defined in Section 3.

5.1 Simulated CIR

We have shown in Fig. 5 the simulated impulse responses of the LOS path and those corresponding to one, two, and three reflections for the case of medium-size room. Note that the levels of different LOS components are indicated by labels for the purpose of illustration. R_1 and R_3 positions are considered together with the two cases of blocked LOS and tilted receiver for the latter. For the tilted receiver case, we consider a tilting angle of 30° towards the centre of the ceiling (an untilted receiver points vertically towards the ceiling). This way, we have different LOS paths and also additional reflections from the floor and walls.

At R_1, concerning the LOS component, we notice a single shifted Dirac delta function from Fig. 5*a*, which is due to the symmetry of the LED arrangement with respect to the receiver position in this case (see Fig. 3). There are three shifted Diracs at R_3 (except for the blocked-LOS case), where we have a symmetry with respect to LEDs 1 and 4. It is worth mentioning that since the LOS paths dominate the diffuse component in the CIR, they are the main factor that determines the channel frequency selectivity. Lastly, we have an almost similar behaviour for the cases of tilted and untilted receivers as in Figs. 5*b* and *d*, apart from the received intensity level, as expected.

5.2 RMS delay spread

To evaluate the channel frequency selectivity based on the delay spread criterion, we calculate for different scenarios the mean excess delay τ and the RMS delay spread μ using the simulated aggregated CIRs (i.e. taking both LOS and diffuse components into account). At the same time, since both the asymmetry between the LOS paths (if any) and the diffuse component (non-LOS) contribute to the channel frequency selectivity, in order to see the significance of the former factor, we have also calculated τ and μ based only on the LOS component. The results are summarised in Table 2 where the two cases of medium-size and large rooms are considered. We have furthermore shown in the last column of the table the ratio of the total power corresponding to the LOS component to that of the diffuse component; what is usually referred to as 'Rice-factor' in RF systems. Let us focus on the RMS delay spread and the case of

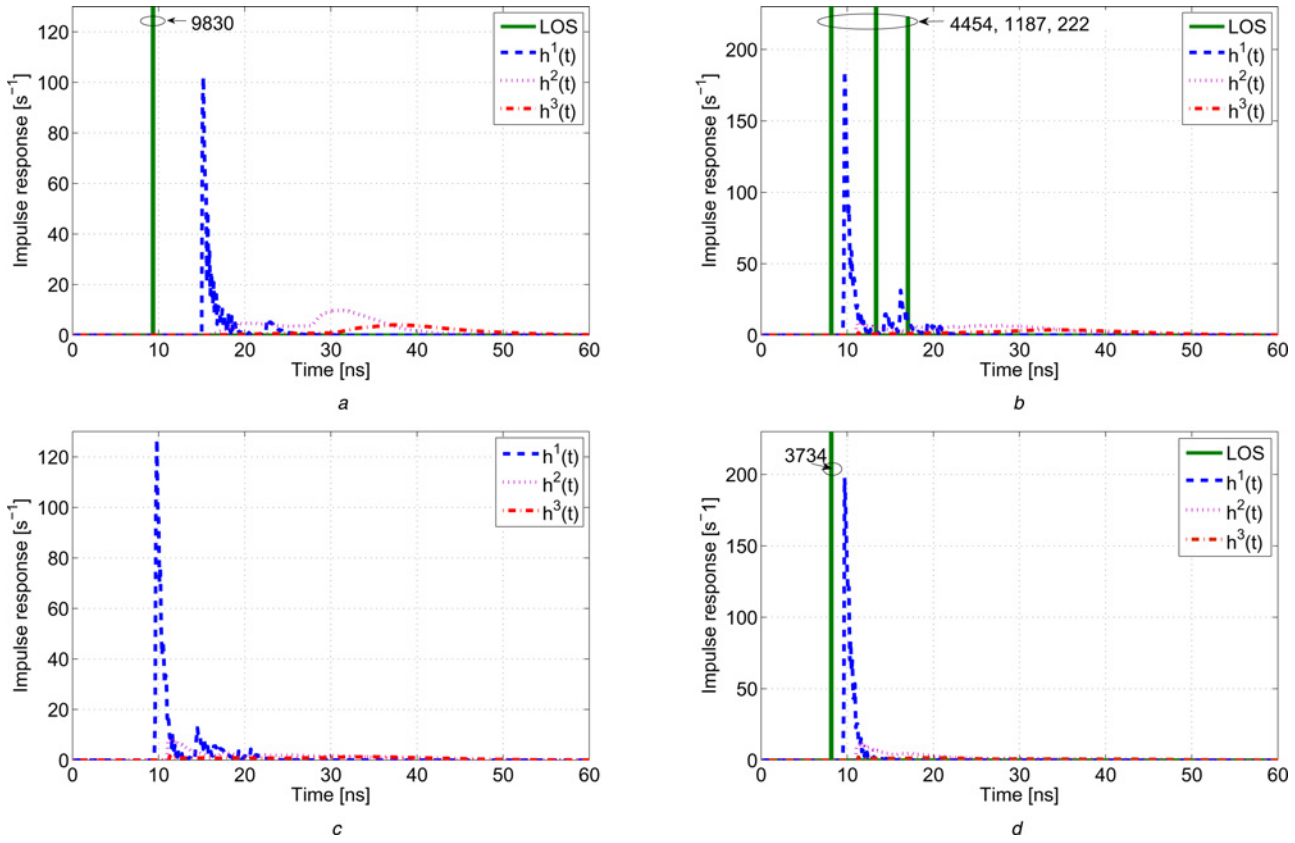

Fig. 5 *Medium-size room case, CIR at receiver positions*

a R_1
b R_3
c R_3, blocked LOS
d R_3, tilted receiver

medium-size room. At R_1, there is no delay spread corresponding to the LOS component due to the symmetry of LEDs arrangement with respect to the receiver position. We notice a larger μ for R_2 and R_3 positions, compared with R_1. The reason is that at these positions we have more asymmetry between the LOS paths and this results in a larger delay spread. We also note a slightly larger μ for the case of tilted receiver, which is quite logical. In fact, for a larger tilting angle, we receive more contribution from the LOS and also from the diffused light due to the reflections from the floor and the walls. Lastly, for the case of blocked LOS, we obtain a relatively large μ of more than 4 ns.

On the other hand, for the case of a large room, we notice generally larger delay spreads. Interestingly, here the major part of μ arises from the contribution of LOS, and taking the diffuse component into account affects the delay spread only slightly. As a matter of fact, the more significant factor affecting μ is the asymmetry between the multiple LOS paths (16 in total for the large room case). As expected, again the largest delay spread corresponds to the room corner, that is, R_3' position.

As a matter of fact, although the study of the RMS delay spread seems to be useful in comparing the degree of channel frequency selectivity of the different link configurations, its absolute value cannot be used to determine the limitation on the transmission rate. For instance, for the case of the medium-size room at R_3 position, a μ of 1.76 ns would suggest that we can transmit with up to a rate of ~500 Mbps with OOK signalling. However, as we will show later in Section 5.4, the data rate is much more constrained. To this reason, we investigate other metrics in the following.

Table 2 Mean excess delay and RMS delay spread for different link scenarios

	Receiver position	RMS delay spread μ, ns		Rice factor
		LOS	Aggregate channel	
medium-size room	R_1	0	0.26	3.56
	R_2	1.53	1.58	2.90
	R_3	1.69	1.76	1.43
	R_3, blocked LOS	0	4.37	0
	R_3, tilted	2.08	2.15	2.59
large room	R_1'	1.83	2.00	6.53
	R_2'	2.43	3.07	2.96
	R_3'	3.37	4.66	0.89

'LOS' refers to considering only the LOS component of CIR, whereas 'Aggregate channel' includes both LOS and diffuse components.

5.3 Channel frequency response

Let us now investigate the usefulness of the channel frequency response for evaluating the degree of channel frequency selectivity. We have presented in Fig. 6 plots of normalised modulus of channel frequency response for the case of medium-size room at receiver positions R_1, R_2, and R_3 (untilted and tilted receiver, and blocked LOS), as well as for the case of the large room at R_3' position.

First, we notice that for R_1 position, the frequency response is almost flat except for data rates lower than about 30 MHz, which confirms the results of Fig. 5: here, the dominant factor is the LOS component, which is a single shifted Dirac delta function. Thus, it is quite reasonable to have an almost flat frequency response. However, we cannot determine an explicit limitation on the data

IET Optoelectron., 2016, Vol. 10, Iss. 3, pp. 80–88

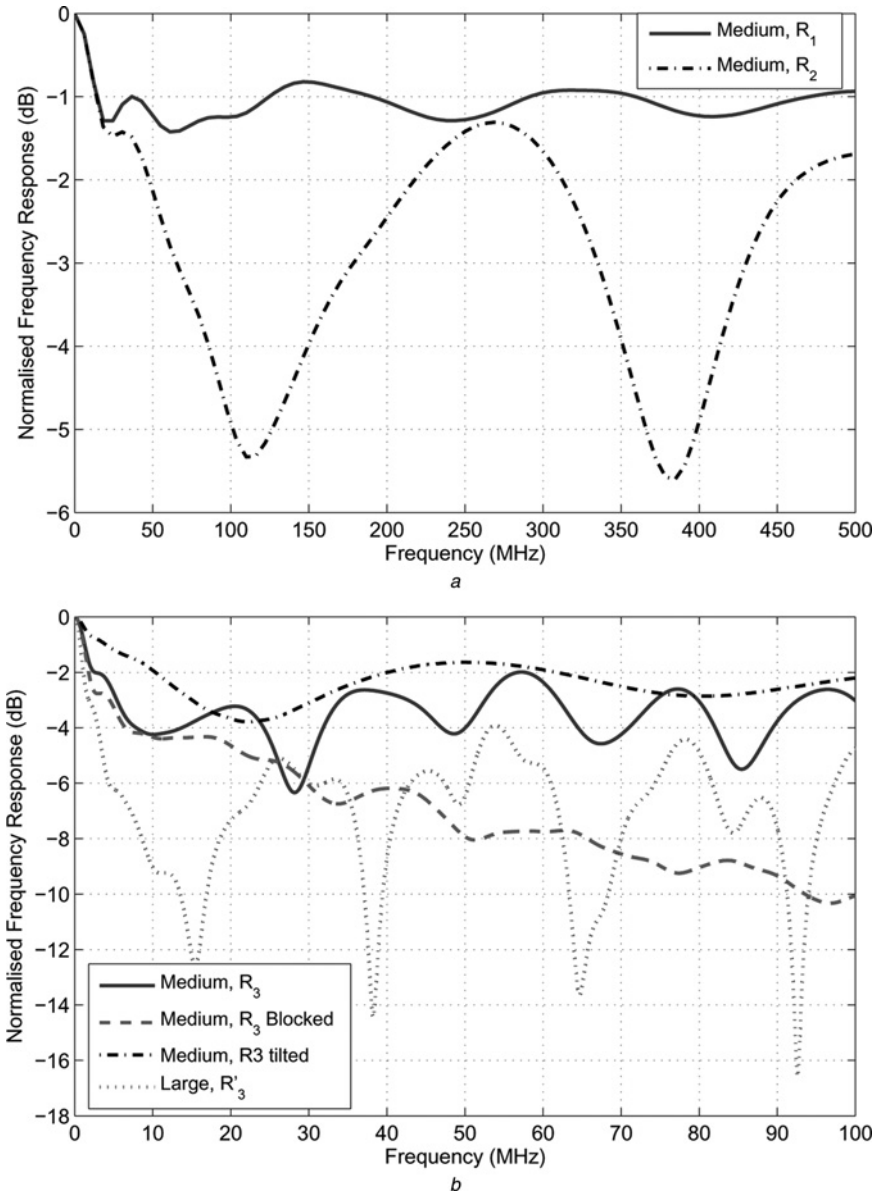

Fig. 6 *Plots of normalised modulus of channel frequency response*

a Medium-size room with receiver at positions R_1 and R_2
b Medium-size room at R_3 position for untilted and tilted receivers and blocked-LOS cases, and large room at position R'_3

rate based on the frequency response. For the cases of R_2 and R_3 positions, we notice oscillations of a few decibels. Once again, the dominant factor is the LOS component of CIR, and since we have three shifted Dirac delta functions (see Fig. 5), we have an oscillating behaviour in the frequency response. From Fig. 6*b*, we notice a somehow similar behaviour for the case of tilted receiver at R_3. For the case of R'_3 position in the large room, we notice more significant fluctuations (in amplitude) in the frequency response. The reason is the contribution of the 16 LOS paths of different delays to the CIR; as a result, in certain frequencies we experience more severe 'fades', compared with the previous cases for the medium-size room.

For all these studied cases, because of the oscillating behaviour of the frequency response (which is due to the contribution of the LOS component), fixing a 3 dB bandwidth for the channel is effectively useless. The 3 dB bandwidth becomes meaningful only for the purely diffuse channel in the case of blocked LOS at R_3 position, which is about 43 MHz. In conclusion, due to the limited interest of the frequency response and the 3 dB channel bandwidth, we resort to the third criterion, that is, SIR, in the following subsection.

5.4 Signal-to-ISI ratio

As mentioned previously, the interest of studying the SIR is that we can predict whether or not a channel equalisation is necessary for a given transmission rate. To evaluate the SIR, for the sake of simplicity, we consider the NRZ OOK modulation. We obtain the received signal by convolving the transmitted OOK signal with the CIR and the receiver filter impulse response. Then, we calculate the SIR numerically using (8). Here, a_j, that is, the 'desired' signal sample is that corresponding to the highest amplitude. In other words, we assume perfect synchronisation at the receiver where received pulses are sampled at their maximum [18]. Note that this does not happen in practice as we cannot predict the exact sampling time, for instance, due to the imperfect knowledge of the CIR, the receiver noise, and the clock frequency jitter of the transmitter and the receiver. The results we present, hence, provide an optimistic estimation of the SIR.

Concerning the receiver filter, we consider the two cases of MF and a BF, as mentioned before. For the latter, we consider a fifth-order BF and set its 3 dB bandwidth to $R_b/2$, where R_b is the symbol rate since it results in the best SNR at the filter output [18].

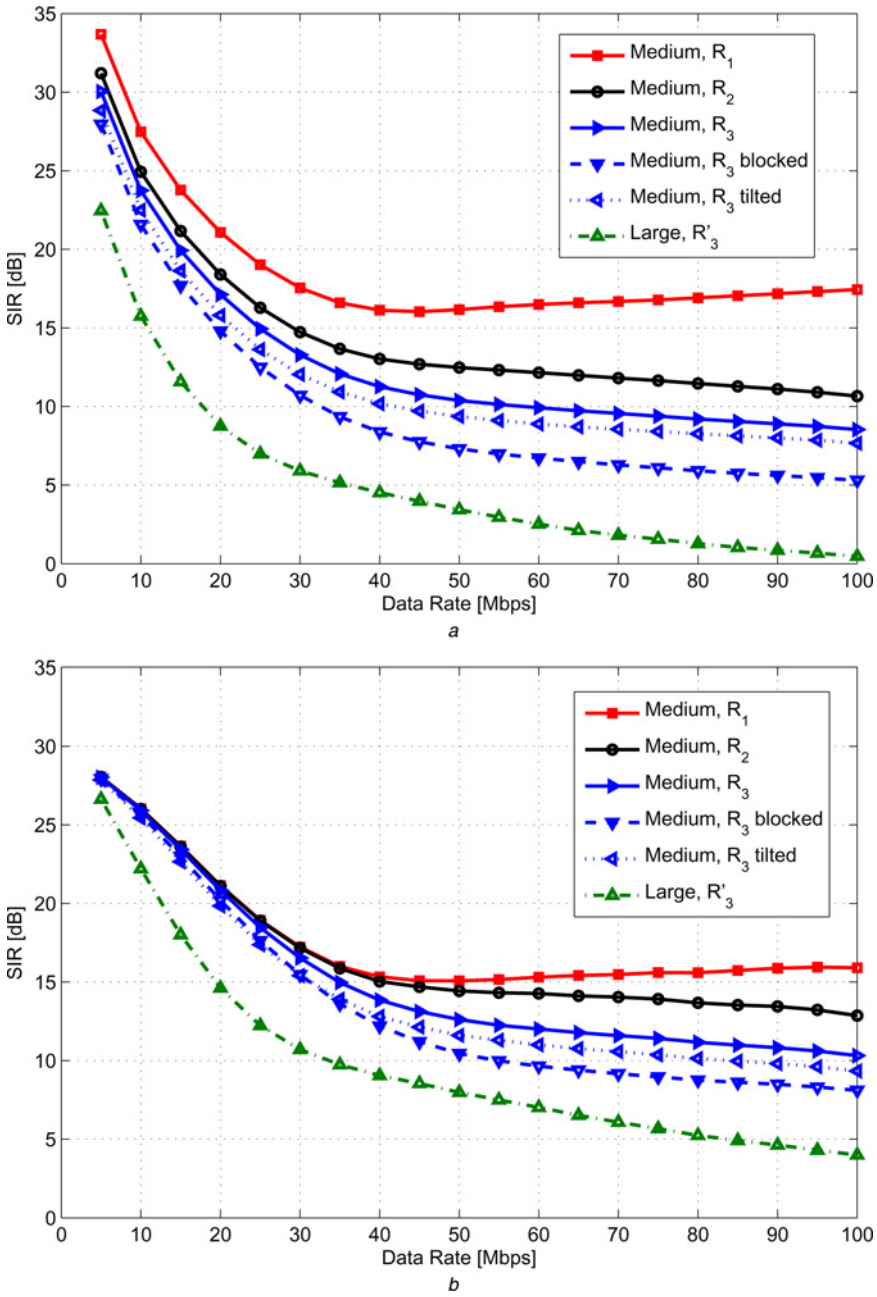

Fig. 7 *SIR as a function of data transmission rate assuming simple OOK signalling while taking into account the effect of*

a Matched filter
b Bessel filter

We have presented plots of SIR as a function a transmission data rate in Figs. 7*a* and *b* for the two cases of MF and BF, respectively. Generally, SIRs are relatively high for data rates lower than 10 Mbps, which means that we have effectively a flat channel. It is quite reasonable since the channel delay dispersion becomes negligible, compared with the symbol duration T_s. Note that for the case of MF, the SIR tends to infinity when data rate tends to zero. This is not the case, however, for the BF, since it does not fully satisfy the Nyquist criterion and introduces a small amount of ISI in the received signal [31].

We notice from the presented results a decrease in SIR as the data rate increases. Interestingly, this is not the case for R_1 position in the medium-size room: we notice an increase in SIR for data rates higher than about 40 Mbps. We can explain this phenomenon by considering the corresponding frequency response in Fig. 6*a*: given that the frequency response is almost flat at high frequencies, we suffer from less distortion when shifting to larger bandwidths, that is, high data rates. In other words, we can consider the diffuse component of the CIR as a 'low-pass' component that we can neglect at high frequencies, where the LOS component dominates. Note that this is also true for the other case studies but the particularity of R_1 position is that due to the symmetry in the LED lamp arrangement, we have one single Dirac as the LOS component of CIR. For the other cases, the existence of several Dirac functions in the CIR determines the SIR limitation at high data rates.

From Fig. 7, the worst SIR corresponds to the case of R_3' in the large room where the limitation on the SIR arises from the numerous (i.e. 16) LOS paths that contribute to ISI at relatively high data rates. For the medium-size room, the case of blocked LOS at R_3 is reasonably much more constraining than the unblocked cases. These results are in accordance with the conclusions of the previous subsections.

Another interesting point is that SIRs are generally higher when using a BF (except at relatively low data rates <10 Mbps for

IET Optoelectron., 2016, Vol. 10, Iss. 3, pp. 80–88

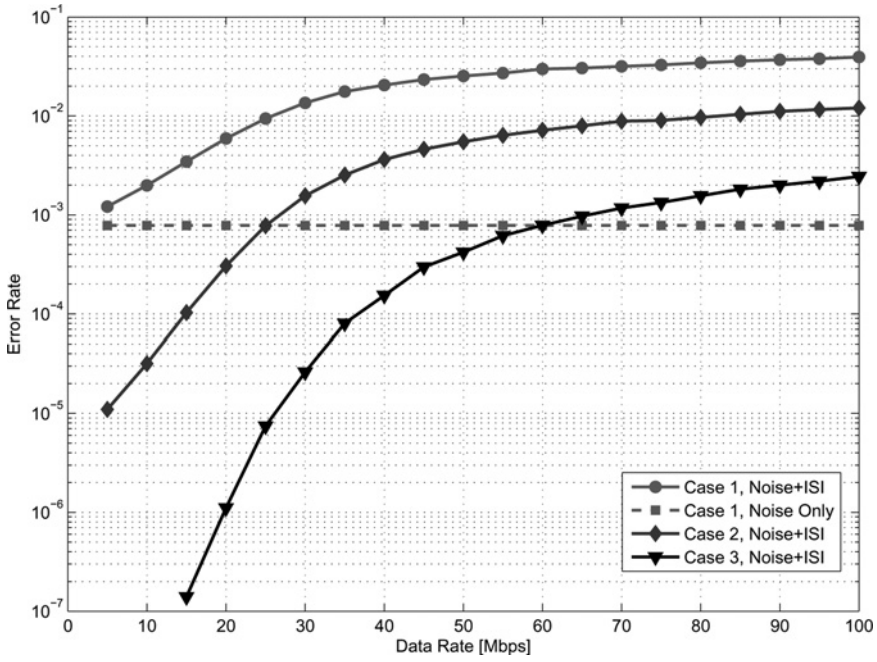

Fig. 8 *Receiver BER as a function of the data transmission rate for* R_3 *position in the medium-size room. OOK modulation with MF at the receiver; case 1:* $E_b/N_0 = 10$ *dB, case 2:* $E_b/N_0 = 13$ *dB, case 3:* $E_b/N_0 = 16$ *dB*

medium-size room). As a matter of fact, as mentioned previously, the BF does not fully satisfy the Nyquist criterion and introduces an vertical eye-opening penalty of about 0.9 dB in the electrical domain for $h(t) = \delta(t)$, compared with the MF. However, the shape of the eye is significantly flatter near the sampling time. As a result, the BF is more tolerant to sampling time errors than the MF. For the same reason, it is also more robust against multipath dispersion.

Lastly, it is worth mentioning that at relatively high data rates (here, about more than 5 Gbps), the SIR tends to an asymptotic value. Indeed, by increasing the data rate, the transmitted pulses become more and more narrow, and at the limit, the received signal approaches the CIR. This asymptotic value of SIR can be validated from the CIR results.

5.5 Error rate

To get more insight into the real impact of the ISI on the system performance, let us investigate the system bit-error-rate (BER). Assuming signal-independent AWGN of double-sided PSD $N_0/2$, we consider three case studies where we fix the electrical E_b/N_0 to 10, 13, and 16 dB. We will refer to them as cases 1, 2, and 3, respectively. Here, E_b is the average received electrical energy per bit. We consider OOK modulation with MF at the receiver. We assume perfect time synchronisation and channel knowledge at the receiver, which means that we consider signal sampling at optimal points and set the optimal threshold for OOK signal detection. This way, for the case of a 'ideal' flat channel (i.e. with CIR of one single Dirac), the BER is given by

$$P_b = \frac{1}{2} \cdot \mathrm{erfc}\left(\sqrt{\frac{E_b}{2N_0}}\right). \tag{13}$$

This equals 7.83×10^{-4}, 3.97×10^{-6}, 1.4×10^{-10} for cases 1, 2, and 3, respectively. Assuming rectangular NRZ pulse shaping at the transmitter, the mean optical transmit power P_T is related to E_b according to the following equation

$$P_T = \sqrt{\frac{E_b R_b}{2}}, \tag{14}$$

where we have normalised the received signal with respect to the PD responsivity and TIA gain, for simplicity. Results are shown in Fig. 8, where we have presented plots of BER as a function of the data rate for the case of R_3 receiver position for the medium-size room. The case of 'ideal' flat channel, denoted by 'Noise Only' on the figure, serves as the benchmark, for which the BER remains unchanged, irrespective of the data rate. The plots denoted by 'Noise+ISI' correspond to the real channel and are obtained through Monte Carlo simulations. We can clearly notice the BER penalty due to ISI; this penalty becomes logically more important by increasing the data rate. For instance, if we consider a target BER of 7.83×10^{-4} (from case 1, Noise Only), we have no ISI penalty at ~1 Mbps (from case 1, Noise+ISI); a 3 dB SNR penalty at ~25 Mbps (from case 2, Noise+ISI), and a 6 dB SNR penalty at ~60 Mbps (from case 3, Noise+ISI). These results are in accordance with those of Fig. 7, that is, we suffer from more and more ISI by increasing the data rate.

6 Conclusion

Using the iterative site-based method, we simulated the impulse response of the aggregated indoor VLC channel for different scenarios, and then investigated the necessity of channel equalisation at the receiver. We showed that channel frequency selectivity arises mainly from the multiple LOS paths rather than diffuse propagation, that is, multipath reflections. It can be relatively significant for large rooms where numerous LED lamps are used for illumination. Hence, the argument that is commonly presented in the literature according to which 'when a LOS exists, the channel can mostly be considered as frequency non-selective,' should be used with prudence. We demonstrated the interest of the proposed SIR in determining the degree of channel frequency selectivity. Meanwhile, we discussed the choice of the receiver filter and demonstrated the interest of using a Bessel low-pass filter, which provides a higher SIR at relatively high data rates, compared with the MF, for instance. The impact of the channel frequency selectivity was also demonstrated through numerical results on the receiver error rate.

7 Acknowledgments

The authors thank Dr Laurent Ros from GIPSA-lab, Grenoble, France, for the valuable comments and inspiring ideas. They also acknowledge the support provided by the EU Opticwise COST Action IC1101. Parts of this work were presented in the International Workshop on Optical Wireless communications (IWOW), 2014, Madeira, Portugal [32].

8 References

1 Grobe, L., Paraskevopoulos, A., Hilt, J., *et al.*: 'High-speed visible light communication systems', *IEEE Commun. Mag.*, 2013, **51**, (12), pp. 60–66
2 Jovicic, A., Li, J., Richardson, T.: 'Visible light communication: opportunities, challenges and the path to market', *IEEE Commun. Mag.*, 2013, **51**, (12), pp. 26–32
3 Ghassemlooy, Z., Minh, H.L., Haigh, P.A., *et al.*: 'Development of visible light communications: emerging technology and integration aspects'. Optics and Photonics Taiwan Int. Conf. (OPTIC), Taipei, Taiwan, December 2012
4 Grobe, L., Langer, K.-D.: 'Block-based PAM with frequency domain equalization in visible light communications'. IEEE Global Communication Conf. (Globecom), Atlanta, GA, December 2013, pp. 1070–1075
5 Zhang, S., Watson, S., McKendry, J.J.D., *et al.*: '1.5 Gbit/s multi-channel visible light communications using CMOS-controlled GaN-based LEDs', *J. Lightwave Technol.*, 2013, **31**, (8), pp. 1211–1216
6 Tsonev, D., Chun, H., Rajbhandari, S., *et al.*: 'A 3-Gb/s single-LED OFDM-based wireless VLC link using a gallium nitride μled', *IEEE Photonics Technol. Lett.*, 2014, **26**, (7), pp. 637–640
7 Grubor, J., Randel, S., Langer, K.-D.D., *et al.*: 'Broadband information broadcasting using LED-based interior lighting', *IEEE/OSA J. Lightwave Technol.*, 2008, **26**, (24), pp. 3883–3892
8 Armstrong, J.: 'OFDM for optical communications', *J. Lightwave Technol.*, 2009, **27**, (3), pp. 189–204
9 Lee, S.C.J., Randel, S., Breyer, F., *et al.*: 'PAM-DMT for intensity-modulated and direct-detection optical communication systems', *IEEE Photonics Technol. Lett.*, 2009, **21**, (23), pp. 1749–1751
10 Dimitrov, S., Sinanovic, S., Haas, H.: 'Signal shaping and modulation for optical wireless communication', *J. Lightwave Technol.*, 2012, **30**, (9), pp. 1319–1328
11 Azhar, A.H., Tran, T.-A., Obrien, D.: 'A gigabit/s indoor wireless transmission using MIMO-OFDM visible-light communications', *IEEE Photonics Technol. Lett.*, 2013, **25**, (2), pp. 171–174
12 Elgala, H., Little, T.D.C.: 'Reverse polarity optical-OFDM (RPO-OFDM): dimming compatible OFDM for gigabit VLC links', *Optics Express*, 2013, **21**, (20), pp. 24288–24299
13 Vucic, J., Kottke, C., Nerreter, S., *et al.*: '513 Mbit/s visible light communications link based on DMT-modulation of a white LED', *J. Lightwave Technol.*, 2010, **28**, (24), pp. 3512–3518
14 Khalid, A.M., Cossu, G., Corsini, R., *et al.*: '1-Gb/s transmission over a phosphorescent white LED by using rate-adaptive discrete multitone modulation', *IEEE Photonics J.*, 2012, **4**, (5), pp. 1465–1473
15 Cossu, G., Khalid, A., Choudhury, P., *et al.*: '3.4 Gbit/s visible optical wireless transmission based on RGB LED', *Opt. Express*, 2012, **20**, (26), pp. B501–B506
16 Armstrong, J., Schmidt, B.J.C.: 'Comparison of asymmetrically clipped optical OFDM and DC-biased optical OFDM in AWGN', *IEEE Commun. Lett.*, 2008, **12**, (5), pp. 343–345
17 Wolf, M., Cheema, S.A., Haardt, M., *et al.*: 'On the performance of block transmission schemes in optical channels with a Gaussian profile'. Int. Conf. on Transparent Optical Networks (ICTON), Graz, Austria, July 2014, pp. 1–8
18 Wolf, M., Grobe, L., Rieche, M.R., *et al.*: 'Block transmission with linear frequency domain equalization for dispersive optical channels with direct detection'. Twelfth IEEE Int. Conf. on Transparent Optical Networks (ICTON), Munich, Germany, June 2010, pp. 1–8
19 Wu, F.-M., Lin, C.-T., Wei, C.-C., *et al.*: '1.1-Gb/s white-LED-based visible light communication employing carrier-less amplitude and phase modulation', *IEEE Photonics Technol. Lett.*, 2012, **24**, (19), pp. 1730–1732
20 Wu, F.-M., Lin, C.-T., Wei, C.-C., *et al.*: 'Performance comparison of OFDM signal and CAP signal over high capacity RGB-LED-based WDM visible light communication', *IEEE Photonics J.*, 2013, **4**, (4), id 7901507
21 Wolf, M., Cheema, S.A., Khalighi, M.A., *et al.*: 'Transmission schemes for visible light communication in multipath environments'. Int. Conf. on Transperent Optical Networks (ICTON), Budapest, Hungary, July 2015
22 Carruthers, J.B., Kannan, P.: 'Iterative site-based modeling for wireless infrared channels', *IEEE Trans. Antennas Propag.*, 2002, **50**, (5), pp. 759–765
23 Lee, K., Park, H., Barry, J.R.: 'Indoor channel characteristics for visible light communications', *IEEE Commun. Lett.*, 2011, **15**, (2), pp. 217–219
24 Jungnickel, V., Pohl, V., Noenning, S., *et al.*: 'A physical model of the wireless infrared communication channel', *IEEE J. Sel. Areas Commun.*, 2002, **20**, (3), pp. 631–640
25 Kahn, J.M., Barry, J.R.: 'Wireless infrared communications', *Proc. IEEE*, 1997, **85**, (2), pp. 265–298
26 Komine, T., Nakagawa, M.: 'Fundamental analysis for visible-light communication system using LED lightings', *IEEE Trans. Consum. Electron.*, 2004, **50**, (1), pp. 100–107
27 Personick, S.D.: 'Receiver design for optical fiber systems', *Proc. IEEE*, 1977, **65**, (12), pp. 1670–1678
28 Ghassemlooy, Z., Popoola, W., Rajbhandari, S.: 'Optical wireless communications: system and channel modelling with MATLAB' (CRC Press, 2013)
29 Rahaim, M., Little, T.D.C.: 'SINR analysis and cell zooming with constant illumination for indoor VLC networks'. Int. Workshop on Optical Wireless Communications (IWOW), Pisa, Italy, October 2012, pp. 20–24
30 Zeng, L., O'Brien, D.C., Le Minh, H., *et al.*: 'High data rate multiple input multiple output (MIMO) optical wireless communications using white LED lighting', *IEEE J. Sel. Areas Commun.*, 2009, **27**, (9), pp. 1654–1662
31 Proakis, J.G., Salehi, M.: 'Digital communications' (McGraw-Hill, New York, 2007, 5th edn.)
32 Long, S., Khalighi, M.A., Wolf, M., *et al.*: 'Channel characterization for indoor visible light communications'. Int. Workshop on Optical Wireless Communications (IWOW), Madeira, Portugal, September 2014, pp. 75–79